

Characteristics of Flame-Nucleated Carbonaceous Nanoparticles

Francesca Picca^{*a}, Gianluigi De Falco^a, Mario Commodo^b,
Giuseppe Vitiello^a, Gerardo D'Errico^c, Patrizia Minutolo^b, Andrea D'Anna^a

^a Dipartimento di Ingegneria Chimica, dei Materiali e della Produzione Industriale - Università degli Studi di Napoli Federico II, P.le Tecchio 80, 80125, Napoli, Italy

^b Istituto di Ricerche sulla Combustione - CNR, P.le Tecchio 80, 80125, Napoli, Italy

^c Dipartimento di Scienze Chimiche - Università degli Studi di Napoli Federico II, Complesso Monte S. Angelo, 80126, Napoli, Italy

francesca.picca@unina.it

Flame-formed just-nucleated carbon nanoparticles, with sizes of about 2-10 nanometers, have been the object of increasing interest over the last decades not only because of environmental concerns but also as new procedure for synthesis of engineered nanoparticles. In this work, we present an experimental study on synthesis and characterization of carbon nanoparticles generated in a laminar premixed ethylene/air flame. The production of carbon nanoparticles of different sizes and properties is achieved by changing the particle residence time in the flame, i.e., collecting the carbon nanoparticles at different heights above the burner. Particle size distributions, Raman, UV-visible and electron paramagnetic resonance (EPR) spectroscopies have been used to characterize the sampled particles. The size of the particles increases as the residence time in the flame increases, the particle size distributions changing from a unimodal to bimodal. Chemical and structural modifications are retrieved by Raman and EPR analysis. Raman spectra show the G and D bands, typical of disordered carbonaceous materials. Their relative intensity and band position changes during the growing process and are used as index of structural changes. EPR spectroscopy, a powerful tool to probe electronic properties of carbon-based materials, reveals the presence and superposition of multiple paramagnetic species. Persistent carbon-centered aromatic radicals are detected for all the sampled particles and an abrupt change in the EPR signal is observed as the particle distribution changes from monomodal to bimodal. EPR indicate a three-dimensional structural organization when larger particles are formed. Optical properties are retrieved by UV-visible spectroscopy which, combined to Raman and EPR spectroscopy, seems to be powerful diagnostics to monitor particle clustering and to control the process of engineered carbonaceous nanoparticle production.

1. Introduction

Just-nucleated carbon nanoparticles, CNPs, in flame have been the object of several studies in the last decades. Most of these studies have been driven by human health and environmental/climate change issues (Bond et al., 2013; De Falco et al., 2017; Gualtieri et al., 2008). These nanoparticles have also aroused the interest of scientific community because of the possibility to use them as potential new low-cost materials with a very large application fields (Li et al., 2016). Under controlled synthesis conditions, these CNPs may be produced and functionalized to form desirable materials. The CNPs synthesis process, from the incomplete combustion of hydrocarbons, start with the formation of polycyclic aromatic hydrocarbon (PAH), high molecular mass compounds that act as particle precursors. During the growing process, PAHs begin to assemble into clusters of few nanometers size, i.e., 2-3 nm (Commodo et al., 2018), which growth to larger particles changing the residence time in the flame reactor.

In this study, CNPs have been generated in a laminar premixed ethylene/air flame with an atomic ratio C/O = 0.67 (equivalence ratio $\Phi = 2.03$). The physicochemical characterization of the CNPs is performed on-line by differential mobility analysis (DMA), to gain information about change in particle size distributions (PSDs) as a

function of different heights above the burner (HABs), and off-line by Raman spectroscopy, UV-visible spectroscopy and electron paramagnetic resonance (EPR) spectroscopy, in order to gain structural and chemical information on the synthesized nanoparticles. The aim of this research is to study structural, chemical and optoelectronic properties of the flame-formed CNPs to pave the way for a better control on the process of engineered carbonaceous nanoparticle production.

2. Experimental

A premixed laminar ethylene-air flame was stabilized on a water cooled sintered bronze McKenna burner. The cold gas stream velocity was 9.8 m/s and the carbon to oxygen (C/O) atomic ratio was set at 0.67, corresponding to a flame equivalence ratio Φ of 2.01. On-line analysis was performed by means of a differential mobility analyzer (DMA) system, more details on the experimental procedure can be found in previous works (Commodo et al., 2015). The combustion products are sampled through a very small orifice, i.e., 200 μm , located on the bottom side of the probe and rapidly mixed with N_2 , thus providing a dilution ratio of 1:3000 that prevents particles from coagulating and allows quenching of the chemical reactions throughout the sampling line (Commodo et al., 2016). Off-line analyses were performed on particles sampled with a tubular probe (similar to the one used for PSDs measurements) and collected on quartz filters (Whatman QM-A Quartz Microfiber Filters, with diameter of 47 mm) placed on-line in a filter holder (Shulz et al., 2018). Total sampling time for each filter was about 7 hours. Particles collected on the Quartz filters were then analyzed by Raman spectroscopy using a Horiba XploRA Raman microscope system equipped with a 100 \times objective (NA0.9, Olympus). The laser source was a frequency doubled Nd:YAG laser ($\lambda = 532 \text{ nm}$) and an infrared laser ($\lambda = 785 \text{ nm}$). The power of the excitation laser beam, the exposure time and the other instrumental parameters were opportunely adjusted to avoid structural changes of the sample due to thermal decomposition and to ensure the best resolution. Spectra were obtained with a laser beam power of 1 %, and an accumulation exposure time of 5 cycles of 30 s each. Finally, all the spectra were baseline corrected and normalized to the maximum of the G-peak, around 1600 cm^{-1} . In addition, Raman spectra of commercially available carbon-based material have been also measured. These include: carbon black (CB), activated carbon (AC) and defective graphite (DG). UV-visible absorption spectroscopy was performed on CNPs thermophoretically collected on quartz substrates. The UV-visible absorption spectra were recorded with an Agilent UV-Vis 8453 spectrophotometer. The optical band gap, i.e., the energy gap between the highest occupied molecular orbital (HOMO) and lowest unoccupied molecular orbital (LUMO), of the combustion formed particles was determined from the measured absorption spectra using the well know Tauc's procedure. (Tauc et al., 1996). EPR spectroscopy experiments of soot particles collected on the quartz filters were carried out by means of X-band (9 GHz) Bruker Elexys E-500 spectrometer (Bruker, Rheinstetten, Germany), equipped with a super-high sensitivity probe head. Defined sections of quartz filters were coaxially inserted in a standard 8 mm quartz sample tube and the measurements were performed at 25 $^{\circ}\text{C}$. The instrumental settings were as follows: sweep width, 100 G; resolution, 1024 points; modulation frequency, 100 kHz; modulation amplitude, 1.0 G. EPR spectra were recorded at an attenuation value of 15 dB and 128 scans were accumulated to improve the signal-to-noise ratio. The g-factor values were evaluated by means an internal standard (Mg/MnO) (Yordanov and Lubenova, 2000) which was inserted in the quartz tube co-axially with the samples. The quantitative analysis of the EPR spectra was specifically realized by determining the signal line width, ΔB , measured as peak-to-peak distance of the first-derivative signal (instrumental output), while the determination of the Gaussian and Lorentzian contributions to the line-shape was obtained by estimating the $\Delta B_{1/2}/\Delta B$ ratio, where $\Delta B_{1/2}$ is the half-height width of the EPR absorption signal. In all the cases examined in the present work, the line shape features were estimated and reported as percentages of the Lorentzian character (Raquero et al., 1992).

3. Results

Particle size distributions measured by DMA system along the flame axis have been performed and reported in a previous work (Commodo et al., 2015). By increasing the HABs, the PSDs showed an evolution from a unimodal distribution, characterized by a mean particles size between 2 and 3 nanometers, to a bimodal distribution, characterized by the presence of an additional mode in the size range between 4 and 10 nanometers. The shift from unimodal to bimodal distribution occurs between 8 mm and 9 mm. Information on the chemical and structural modification of carbonaceous nanoparticles were obtained by Raman spectroscopy. The Raman spectra of soot were collected in the first order Raman region, comprised between 1000 cm^{-1} and 2000 cm^{-1} , as a function of HABs. Acquired spectra obtained by using two different excitation wavelengths, i.e., $\lambda = 532 \text{ nm}$ and $\lambda = 785 \text{ nm}$, are shown in Figure 1. All the measured spectra present the typical characteristics of any disordered carbonaceous materials for which a thorough description is reported

elsewhere (Minutolo et al., 2014). As Figure 1 shows, all first order spectra present one band centered at about 1600 cm^{-1} named G band, and the other centered at about 1350 cm^{-1} named D band.

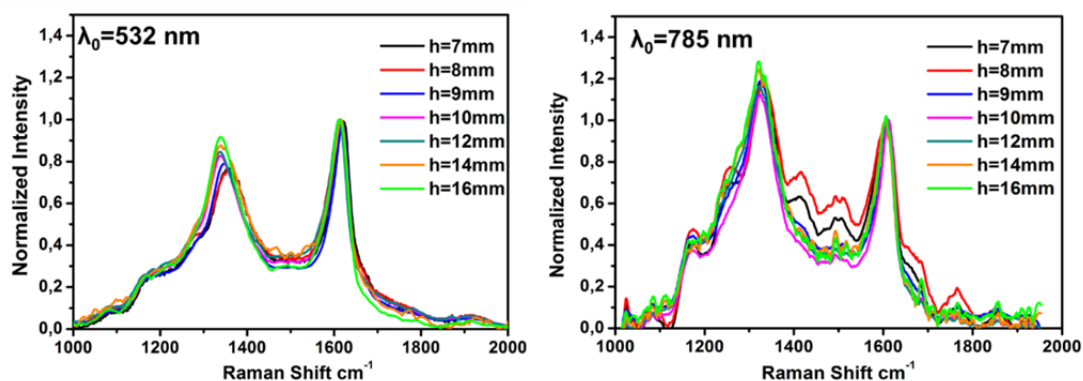


Figure 1: Raman spectra at several heights above the burner. On the left, collected spectra at $\lambda_0=532\text{ nm}$; on the right, collected spectra at $\lambda_0=785\text{ nm}$. The Raman spectra have been normalized on the G peak after subtracting the photoluminescence background.

Activation of the Raman D mode, at $\sim 1350\text{ cm}^{-1}$, is due to the presence of defects in the sp^2 aromatic network, prohibited in the perfect hexagonal lattice (Ferrari and Basko, 2013). Conversely, the G band, at $\sim 1600\text{ cm}^{-1}$, is due to every sp^2 bond and is mostly insensitive to defects. These bands change in width and position of the maximum as function of the different carbon structures. It is worth noticing that spectra show other Raman features as some weak shoulders of D and G bands. The major differences in the spectra of the CNPs as a function of HABs consist in changes in the relative intensity of the D and G peaks and in the bands position. With regard to relative intensity, at $\lambda_0=785\text{ nm}$ the D band intensity is greater than G band one. The dependence of the $I(D)/I(G)$ ratio on the photon energy of the excitation beam is caused by a deviation of the D band intensity from the dependence predicted by the Raman scattering. This is because, unlike G, D band is very sensitive to the resonance Raman effect and the transition probability shows a great dependence on laser excitation energy. The relative intensity of the D and G band ratio, i.e., $I(D)/I(G)$ is shown in Figure 2.

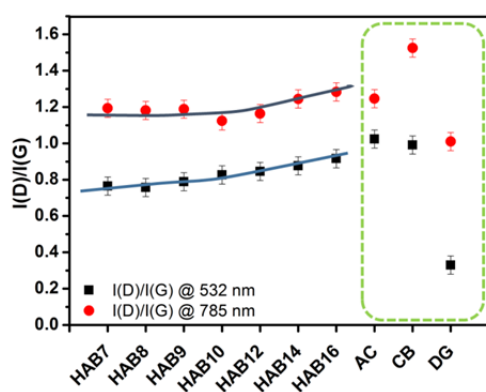


Figure 2: $I(D)/I(G)$ ratio of soot particles collected at several HABs and carbon-based materials

To better understand the shown trends, commercial carbon black (CB), activated carbon (AC) and defective graphite (DG) have been also included in Figure 2. AC and CB contain sp^2 domains of different size in the order of few nm. Defective graphite consists in carbon atom vacancies in an otherwise perfect graphite lattice leading to a small amount of disorder made of sp^3 carbon atoms, breaking the contiguity of the aromatic structure. As shown in Figure 2, the $I(D)/I(G)$ ratio of the flame-formed CNPs is slightly increasing with HAB, approaching that of AC and CB, and is strongly different from DG. It is well known that $I(D)/I(G)$ ratio is related to the average size of the aromatic units or clusters forming the carbon materials, L_a (Ferrari and Robertson, 2001). For graphite and nano-graphite the intensity ratio $I(D)/I(G)$ has been shown to be inversely proportional to L_a (Tuinstra and Koenig, 1970). Such functional dependence has been successively verified up to a minimum L_a , of about 2-3 nm, where $I(D)/I(G)$ reaches a maximum value (Ferrari and Robertson, 2001).

When L_a further decreases, $I(D)/I(G)$ decreases to zero. For flame-generated soot particles, the low- L_a regime, i.e., $L_a < 2-3$ nm, usually applies, for which the following empirical expression has been found to correlate L_a with the relative intensity of the Raman bands (Ferrari and Basko, 2013):

$$L_a^2(\text{nm}^2) = 5.4 \cdot 10^{-2} \cdot E_L^4(\text{eV}^4) \frac{I(D)}{I(G)} \quad (1)$$

where E_L is the energy of the incident photon.

According to this equation, the ratio of the two curves in Figure 2 is expected to be equal to the fourth power of the respective photon energy ratio. This is approximately verified by DG whereas CNPs, CB and AC deviate from this trend. Such discrepancy can be indicative of a lowering of the double resonance mechanism in CNPs, CB and AC. Interestingly, such relaxation effect seems to be more evident the higher HAB, and deserve further investigation. It is relevant to note that using excitation wavelength in the visible, about 532 nm, the dependency of $I(D)/I(G)$ on L_a (Eq. 1) has been validated for a large variety of disordered carbon by many investigations (Ferrari and Basko, 2013) and the evaluation of L_a can be considered reliable. The results obtained for the different soot particles, reported in Figure 3, show a slight increase of L_a as function of HAB. This trend is an indication of larger aromatic islands inside particles at increasing residence time.

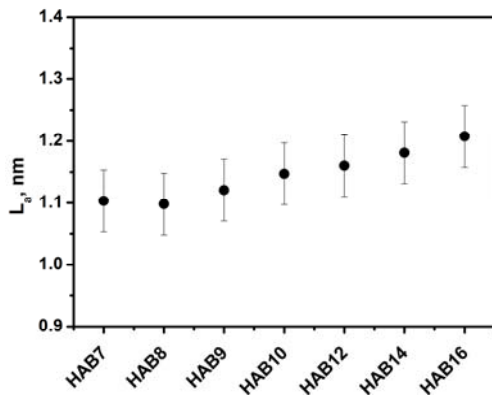


Figure 3: L_a from the Raman spectra of CNPs collected at several HABs.

From UV-visible absorption spectra, Tauc plots have been derived and the values of E_g have been obtained by extrapolation to zero of the linear trend. The plots of $(\text{Abs} \cdot E)^{1/2}$ vs. E , where Abs is the measured absorbance and E is the photon energy, for the particles at HAB= 7 mm, HAB= 9 mm and HAB= 14 mm are reported in Figure 4.

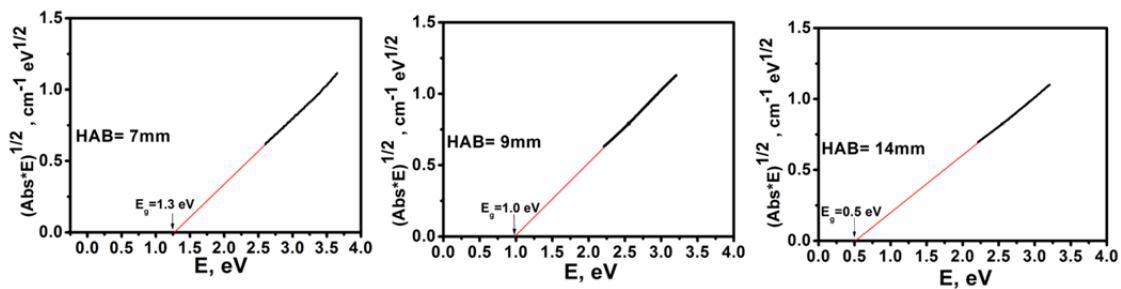


Figure 4: Tauc plots (note: Abs is the measured absorbance and E is the photon energy) and related energy of band gap values of CNPs at: HAB=7 mm, HAB=9 mm, HAB=14 mm.

As reported in Figure 4, the E_g of the CNPs at HAB=7 mm, 9 mm and 14 mm is 1.3 eV, 1.0 eV and 0.5 eV respectively, thus showing a decreasing trend as function of the residence time. This effect can be only partially justified by the increase in the aromatic island length L_a shown in Fig. 3 but it should be also ascribed to the change of particle size, which is increasing from 2-3 nm up to tens of nm.

EPR spectra of soot collected during the growth process are reported in Figure 5 and their relative parameters are reported in Table 1.

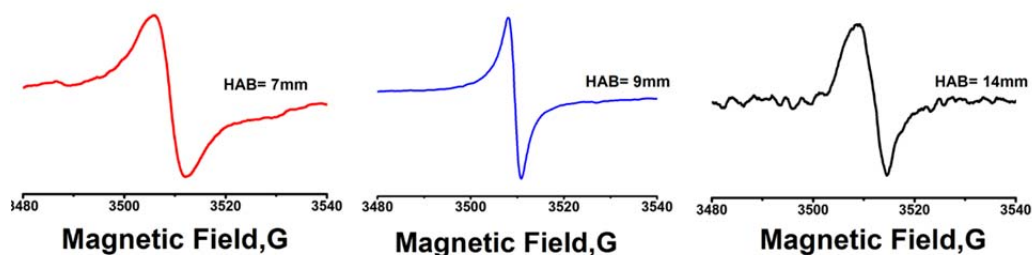


Figure 5: EPR spectra of soot particles on quartz filters at 7 mm, 9 mm and 14 mm.

As reported in a recent work (Vitiello et al., 2018), the EPR spectra of flame-formed CNPs show a single peak at g -factor ranging between 2.0025-2.0028 (± 0.0003). The g -value is defined by the type of radical, i.e. carbon radical, oxygen radical, metal radical, carbon near oxygen radical, and by the chemical environments of unpaired electrons. The obtained value is typical of persistent carbon radicals (Valavanidis et al., 2008). Figure 5 shows a different line-widths of the three signals, also reported in Table 1, suggesting an evolution of the paramagnetic signal as the particle size distribution evolves from monomodal to bimodal. Particularly, particle evolution from 7 mm to 9 mm is characterized by the narrowing of the EPR spectrum while the spectrum recorded at 14 mm is characterized again by a broader signal. There is a correspondence between width and type of the lineshape: broad signal with Gaussian and narrow signal with Lorentzian. The broad lineshape, i.e. Gaussian contribution, of the 7mm sample could be due to the presence and superposition of not interacting unpaired electrons into the particles (Herring et al., 2013). Conversely, the narrow signal of the 9 mm sample, associated to a high Lorentzian contribution, is related to the interaction between unpaired electrons (Ingram, 1958) and indicate the change in the structural organization as due to delocalization of π -electrons (Pilawa et al., 2005). These electrons can interact to form more ordered, stacked structures in a three-dimensional organization (Vitiello et al., 2018). At higher HAB the modified structures of particles due to coagulation/coalescence and surface mass addition lead to a new organization of paramagnetic centres, causing the signal broadening at 14 mm, as shown in Figure 5.

Table 1: EPR spectral parameters of soot particles collected at different HABs.

HAB, mm	g -factor (± 0.0003)	ΔB (G) (± 0.2)	Lorentzian %
7	2.0027	7.6	38
9	2.0025	2.8	98
14	2.0027	6.2	28

4. Conclusions

In this work, a characterization of carbonaceous particles, produced in a laminar premixed flame has been performed. In order to characterize these compounds, the analytic investigations have comprised PSDs measurements, Uv-vis spectroscopy, Raman analysis and EPR spectroscopy. As the residence time in flame increases, the PSD changes from unimodal to bimodal and the average particle size grow from 2-3 nm up to tens of nm. In addition to the particle size, the nanoparticles go through chemical/structural modifications. The analysis of the measured Raman spectra shows that the two main peaks, the D and G bands, change in terms of relative intensity and band position following the evolution of the soot particles toward a more ordered structure during the growing process. Further details on the structural change and on the evolving organization of nanoparticles have been obtained by EPR and UV-visible data. EPR spectroscopy turned out to be a powerful tool to probe electronic properties of carbon-based materials, revealing the presence and superposition of multiple paramagnetic species. These unpaired electrons have a key role in structural organization of materials. Persistent carbon-centered aromatic radicals are detected for all the sampled particles. Noticing an abrupt change in the EPR signals and parameters, in correspondence of the shift from monomodal to bimodal size distributions and at higher residence time it is possible to hypothesize a more ordered three-dimensional structural organization when larger particles are formed. These structural changes are confirmed by UV-visible spectroscopy and Band Gap analysis, which are sensitive to both size effects and

aromatic growth. These results are useful for a deeper understanding of flame formed CNP properties in the perspective of producing these materials as engineered nanomaterial in various fields.

References

- Bond T.C., Doherty S.J., Fahey D.W., et al., 2013, Bounding the role of black carbon in the climate system: A scientific assessment, *Journal of Geophysical Research: Atmospheres*, 118, 5380–5552.
- Commodo, M., De Falco, G., Bruno, A., Borriello, C., Minutolo, P., D'Anna, A., 2015, Physicochemical evolution of nascent soot particles in a laminar premixed flame: From nucleation to early growth, *Combustion and Flame*, 162, 3854–3863.
- Commodo M., De Falco G., Minutolo P., D'Anna A., 2018, Structure and size of soot nanoparticles in laminar premixed flames at different equivalence ratios, *Fuel*, 216, 456–462.
- Commodo M., De Falco G., Minutolo P., D'Anna A., 2016, Thermophoretic sensors for combustion formed nanoparticles, *Chemical Engineering Transaction*, 47, 25–30.
- De Falco G., Terlizzi M., Sirignano M., Commodo M., D'Anna A., Aquino R.P., Pinto A., Sorrentino R., 2017, Human peripheral blood mononuclear cells (PBMCs) from smokers release higher levels of IL-1-like cytokines after exposure to combustion-generated ultrafine particles, *Scientific Reports*, 7, 43016.
- Ferrari A.C. and Robertson J., 2001, Resonant Raman spectroscopy of disordered, amorphous, and diamondlike carbon, *Physical Review B*, 64, 075414.
- Ferrari and Basko, 2013, Raman spectroscopy as a versatile tool for studying the properties of graphene, *Nature Nanotechnology*, 8, 235–246.
- Gualtieri M., Mantecca P., Corvaja V., Bolzacchini E., Fustella G., Zerbi G., Camatini M., 2008, Fine PM and health: in vitro results, *Chemical Engineering Transaction*, 16, 411–418.
- Herring P., Khachatryan L., Lomnicki S., Dellinger B., 2013, Paramagnetic centers in particulate formed from the oxidative pyrolysis of 1-methylnaphthalene in the presence of Fe(III)2O3 nanoparticles, *Combustion and Flame* 160, 2996–3003.
- Ingram, D.J.E., 1958, *Free radicals as studied by electron spin resonance*. London: Butterworths Scientific Publications, 210.
- Li S., Ren Y., Biswas P., Tse S.D., 2016, Flame aerosol synthesis of nanostructured materials and functional devices: processing, modeling, and diagnostics, *Progress in Energy and Combustion Science*, 55, 1–5 .
- Minutolo P., Commodo M., Santamaria M., De Falco G., D'Anna A., 2014, Characterization of flame generated 2-D carbon nano-disk, *Carbon*, 68, 138–148.
- Pilawa B., Wieckowski A.B., Pietrzak R., Wachowska H., 2005, Multi-Component EPR Spectra of Coals with Different Carbon Content, *Acta Physica Polonica. A*, 108, 403–407.
- Requejo A.G., Gray N. R., Freund H., Thomann H., Melchior M. T., Gebhard L. A., Bernardo M., Pictroski C.F., Hsu C. S., 1992, Maturation of petroleum source rocks. 1. Changes in kerogen structure and composition associated with hydrocarbon generation, *Energy Fuels*, 6, 203.
- Schulz F., Commodo M., Kaiser K., De Falco G., Minutolo P., Meyer G., D'Anna A., Gross L., 2018, Insights into incipient soot formation by atomic force microscopy. *Proceedings of the Combustion Institute*, 2018, article in press, doi: 10.1016/j.proci.2018.06.100.
- Tauc J., Grigorovic R., Vancu A., 1996, *Physica Status solidi*, 15, 627–637.
- Tuinstra F. and Koenig J.L., 1970, Raman spectrum of graphite, *The Journal of chemical physics*, 53, 1126–1130.
- Valavanidis A., Iliopoulos N., Gotsis G., Fiotakis K., 2008, Persistent free radicals, heavy metals and PAHs generated in particulate soot emissions and residue ash from controlled combustion of common types of plastic, *Journal of Hazardous Materials*, 156, 277–284.
- Vitiello G., De Falco G., Picca F., Commodo M., D'Errico G., Minutolo P., D'Anna A., 2018, On the relevance of radicals in carbon clustering and soot inception: a joint EPR and Raman spectroscopy study, *Combustion and Flame*, submitted September 23, 2018.
- Yordanov N.D. and Lubenova S., 2000, Effect of dielectric constants, sample containers dimensions and frequency of magnetic field modulation on the quantitative EPR response, *Analytica Chimica Acta*, 403, 305–313.
- Zhao B., Yang Z., Li Z., Wang H., Wexler A.S., Balthasar M., Kraft M., 2003, Measurement and numerical simulation of soot particle size distribution functions in a laminar premixed ethylene oxygen-argon flame, *Combustion and Flame*, 133, 173–188.